Applied Catalysis B: Environmental 176–177 (2015) 429–435

Contents lists available at ScienceDirect

Applied Catalysis B: Environmental

journal homepage: www.elsevier.com/locate/apcatb

Glycerol electrooxidation on self-supported Pd_1Sn_x nanoparticules

A. Zalineeva[a], A. Serov[b], M. Padilla[b], U. Martinez[b], K. Artyushkova[b], S. Baranton[a], C. Coutanceau[a,*], P.B. Atanassov[b]

[a] Université de Poitiers, IC2MP, UMR CNRS 7285, "Catalysis and Non-conventional Media" Group, 4 Rue Michel Brunet, TSA 51106, 86073 Poitiers cedex 9, France

[b] Department of Chemical and Nuclear Engineering and Center for Emerging Energy Technologies, University of New Mexico, Albuquerque, NM 87131, United States

ARTICLE INFO

Article history:
Received 16 January 2015
Received in revised form 9 April 2015
Accepted 16 April 2015
Available online 17 April 2015

Keywords:
FTIRS
Glycerol
Electrooxidation
Palladium
Tin

ABSTRACT

Active self-supported Pd_1Sn_x catalysts are synthesized by the sacrificial support method. Self-supported Pd_1Sn_x catalysts display porous nanostructured morphologies with surface areas ranging from 25 to 80 $m^2\,g^{-1}$ depending on tin content. The mass activity of Pd in Pd_1Sn_x materials toward glycerol oxidation is as follows: $Pd_1Sn_1 > Pd_1Sn_2 > Pd \approx Pd_1Sn_3$. *In situ* FTIR spectroscopy highlighted the unique catalytic behavior of self-supported PdSn materials, particularly the selectivity toward the formation of carboxylate species as soon as 0.2 V *vs* RHE. It has also been shown that the modification of palladium by tin species led to suppress the dissociative adsorption process of glycerol with C—C bond breaking and to favor the bifunctional mechanism. Due to the oxophilic nature of tin species at the electrode surface, the selectivity is completely shifted toward production of carboxylate species as soon as the beginning of the oxidation onset potential at very low potential (*ca.* 0.45 V *vs* RHE).

1. Introduction

The oxidative conversion of glycerol in electrochemical reactors is as a very promising way for the generation of value added compounds from biodiesel industry waste (*ca.* 10 wt% of glycerol for the transesterification reaction of vegetable oil) [1,2] simultaneously with either energy or hydrogen production, depending on the electrochemical reactor configuration (fuel cell or electrolysis cell, respectively) [3]. In alkaline medium the high activity of palladium for glycerol electrooxidation reaction [4,5] makes this metal a very promising alternative to platinum in terms of cost and availability. Moreover, important enhancement of its activity toward electrooxidation of alcohols in alkaline media can be obtained by addition of a second metal with a promotional effect [6,7]. It has also been shown that modification of palladium by *p*-group atoms changes the reaction pathways, allowing controlling the selectivity of the catalytic material [8–10]. Among the *p*-group elements, tin is known to be a high performance co-catalyst, particularly concerning the ethanol electrooxidation reaction in acidic medium [11]. This property of tin in association with palladium was recently confirmed for the electrooxidation of methanol [12], ethanol [13], and ethylene glycol [14] in alkaline medium. The effect of the modification of palladium by tin on the electrocatalytic oxidation of glycerol deserved to be studied. In addition to composition of the catalysts, morphology and microstructure of the material also has an impact on the catalytic behavior; for example, recently it has been shown that self-supported Pd_xBi catalysts presenting hierarchically controlled structures and morphologies with high mesoporosity led to the formation of microreactors allowing unique catalytic behavior in terms of selectivity [15].

For the present work, Pd_1Sn_x catalysts with different Pd/Sn atomic ratios were synthesized using the sacrificial support method (SSM) [16]. This method leads to self-supported, porous, and nanosized structures, with high surface areas. The microstructure, morphology, and composition of the synthesized materials have been determined by different physicochemical methods (BET, SEM, XPS, and atomic absorption), whereas information about their surface structures were obtained by electrochemical methods. Activity and selectivity toward the glycerol electrooxidation reaction were determined as a function of the electrode potential by cyclic voltammetry and *in situ* Fourier transform infrared spectroscopy (FTIRS). The assignment of the infrared absorption bands was previously confirmed by analytical technique [9,17]. FTIRS is then very convenient for determining the reaction products at the electrode/electrolyte interface and for following the formation and consumption of reactant and adsorbed intermediates. This *in situ* technique allows then comprehensively determining the reaction pathways as a function of the electrode potential.

* Corresponding author. Tel.: +33 549454895; fax: +33 549453580.
E-mail address: christophe.coutanceau@univ-poitiers.fr (C. Coutanceau).

http://dx.doi.org/10.1016/j.apcatb.2015.04.037
0926-3373/

2. Experimental

2.1. Synthesis of self-supported Pd_1Sn_x catalysts

A series of catalysts with various Pd:Sn ratios were prepared by the SSM, which was developed at University of New Mexico [16,18]. A known amount of silica Cab-O-Sil EH-5 (surface area = 400 $m^{-2}\,g^{-1}$) was dispersed in water with an ultrasonic probe. Then, the appropriate amounts of metal precursors K_2PdCl_4 (metal content = 32.5 wt%) and $SnCl_4{\cdot}5H_2O$ (metal content = 33.9 wt%) from Sigma–Aldrich were added to the silica suspension. Total loading of metals on silica was calculated to be 13 wt%. The silica/precursor mixture was allowed to dry overnight. The composite materials were reduced under hydrogen atmosphere (7 mol% H_2) at 300 °C for 2 h. After reduction, silica template was removed by etching in 7 M KOH solution and then repeatedly washed with water until neutral pH was achieved. Nominal Pd to Sn atomic ratios were selected as 1:1, 1:2, and 1:3. The catalysts were denominated as Pd, Pd_1Sn_1, Pd_1Sn_2, and Pd_1Sn_3. The hydrolysis step using 7 M KOH solution led to leaching of tin, so that syntheses of catalysts with low tin atomic ratios (Sn/Pd < 1) were difficult to perform. Moreover, in order to reduce the amount of palladium, cheaper catalysts with higher tin amounts were preferred to carry out this study on glycerol oxidation.

2.2. Physicochemical characterizations

The catalysts were comprehensively characterized by scanning electron microscopy (SEM, Hitachi S-5200 Nano SEM instrument with an accelerating voltage of 10 keV), X-ray photoelectron spectroscopy (XPS, Kratos Ultra DLD spectrometer), atomic absorption (AA) and nitrogen adsorption (N_2-BET method using Micrometrics 2360 Gemini analyzer). SEM provided information about the morphologies of samples and sizes of nanoparticles, while AA and XPS were used to determine the compositions of the samples for comparison with the expected ones. XPS was also used to determine the oxidation states and the eventual interactions between different elements in the materials.

2.3. Electrochemical characterizations

The inks for cyclic voltammetry (CV) experiments were prepared by dispersing 5 mg of catalytic powder in 925 μL of a water/isopropanol (4:1) mixture and 75 μL of Nafion (0.5 wt% from DuPont). Homogeneity of the inks was achieved by means of sonication using an ultrasound probe. Then, 10 μL of the mixture was applied onto a 0.2472 cm^2 geometric surface area glassy carbon disk, for a catalyst loading of 0.2 mg cm^{-2}. The electrochemical analysis of the synthesized material was performed using a Pine Instrument Company electrochemical analysis system. The cyclic voltammetry experiments were performed using a disk electrode rotated at 1300 rpm (revolutions per minute). The electrolyte was 1.0 M KOH saturated with N_2 at room temperature. A platinum wire and a Hg/HgO electrode were used as counter and reference electrodes, respectively, although all potentials are quoted *vs* the reversible hydrogen electrode (RHE). Electrocatalytic measurements were realized in 1.0 M KOH + 0.1 M glycerol solution at a scan rate of 0.02 V s^{-1} at 25 °C. The voltammograms were recorded in the potential range from 0.0 to 1.4 V *vs* RHE. The catalysts were cycled through the potential range several times until stable voltammograms were recorded. To assess the stability of Pd_1Sn_x catalysts, chronoamperometry measurements were performed in the presence of 0.1 M glycerol for 5000 s at a potential of 0.6 V *vs* RHE.

In situ Fourier transform infrared (FTIR) spectroscopy (IRRAS – Nicolet 6700 FT-IR spectrometer with MCT detector) was used to gain insight into the mechanism of the glycerol electrooxidation reaction in alkaline medium on a self-supported Pd_1Sn_1 catalyst. The experimental method was described elsewhere [19].

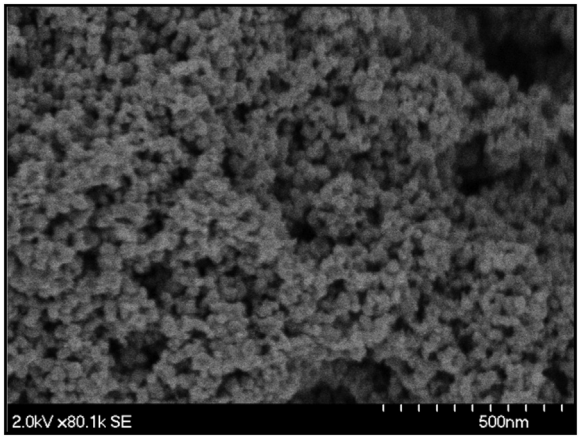

Fig. 1. SEM micrograph for a self-supported PdSn sample.

3. Results

All self-supported Pd_1Sn_x catalysts presented sponge-like structures, as shown in Fig. 1 in the case of Pd_1Sn_1 as an example. SEM image shows the presence of agglomerated nanoparticles with diameter of *ca.* 20 nm, delimiting pores of several tenth nanometers. This hierarchically controlled structure is expected to lead to the presence of pores which could act as nanoreactors for the glycerol electrooxidation as in the case of self-supported Pd_xBi catalysts [15].

The Pd 3d and Sn 3d core level spectra are given in Fig. 2 for each Pd_1Sn_x material used for electrochemical measurements, and Table 1 summarizes the main results of XPS analyses. XPS analyses lean on data from the Handbook of X-ray Photoelectron Spectroscopy [20] and previously published papers [21]. The core level spectrum of Pd 3d 5/2 orbitals shows three symmetrical peaks centered at binding energy values of *ca.* 335, 336, and 337 eV. These peaks are assigned to Pd, $Pd(OH)_2$, and PdO species, respectively.

Table 1
Data from XPS characterization (atomic ratios, binding energy values of XPS peaks related to Pd 3d and Sn 3d, and relative ratios of corresponding Pd and Sn species) of self-supported $PdSn_x$ materials used in electrochemical experiments.

	PdSn		$PdSn_2$		$PdSn_3$	
	Binding energy (eV)	(at.%)	Binding energy (eV)	(at.%)	Binding energy (eV)	(at.%)
Pd^0	335.3	41.0	335.2	54.4	335.5	48.1
$Pd(OH)_x$	336.0	50.6	336.0	38.2	336.0	45.8
PdO	337.4	8.5	337.3	7.4	337.3	6.1
Sn^0	485.1	23.1	485.1	23.3	485.0	23.0
$Sn(OH)_x$	486.6	56.8	486.6	36.7	486.5	51.2
SnO_y	487.3	20.1	488.3	40.0	487.4	25.8

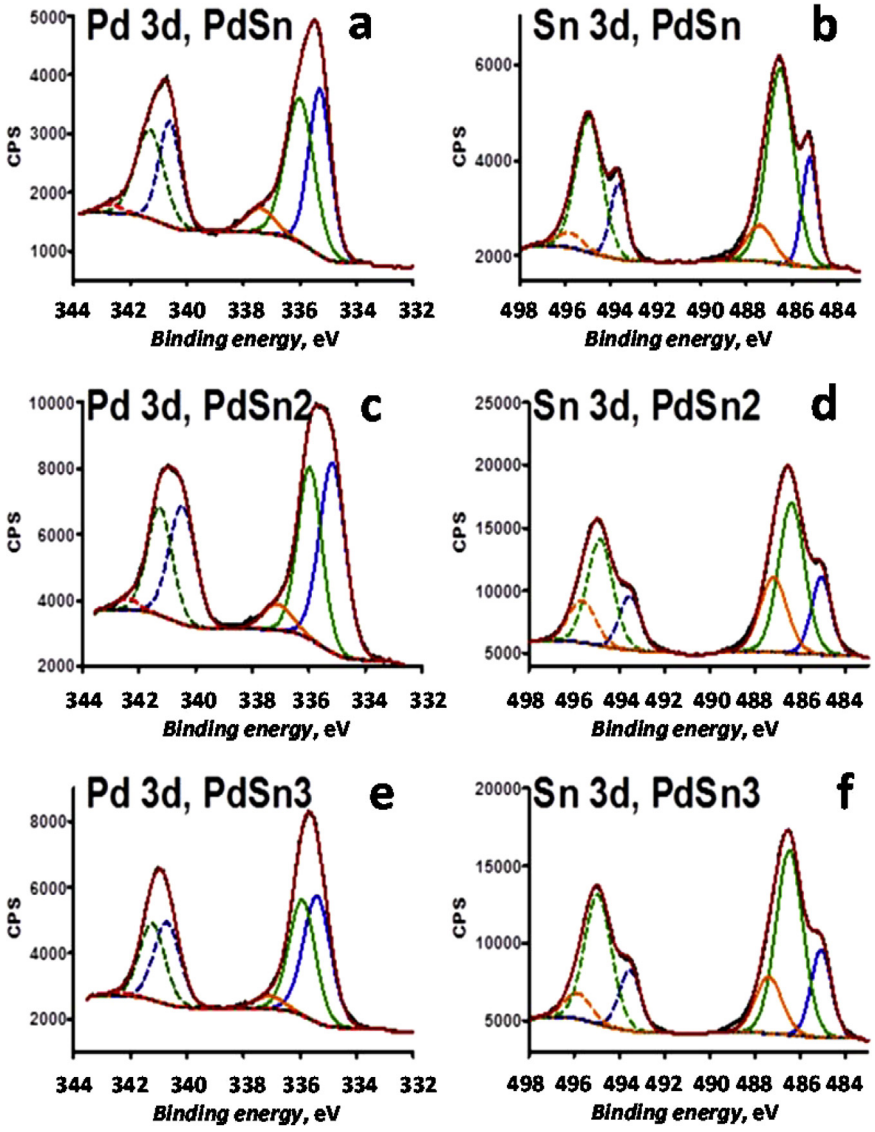

Fig. 2. Detailed XPS core level spectra of Pd 3d and Sn 3d orbitals on synthesized catalysts (a and b) PdSn; (c and d) $PdSn_2$; and (e and f) $PdSn_3$.

The signals corresponding to the Sn 3d 5/2 orbitals could also be accurately convoluted into three peaks centered at binding energy values of *ca.* 485, 486, and 487 eV. Those peaks are assigned to Sn, $Sn(OH)_x$, and SnO_y species, respectively. Table 2 compares Pd/Sn atomic ratios obtained by XPS and AA analyses of the self-supported Pd_1Sn_x catalysts used for electrochemical measurements. The former method is rather a surface analysis method while the latter one is a bulk analysis method. Looking at the AA results, Pd enrichment is observed with regards to the nominal (expected) atomic ratios. Either tin is not incorporated in the material bulk during the thermal reduction step of precursors after the impregnation step of the silica support, or tin is leached from the material during the hydrolysis step by KOH for the removal of the silica template. As a matter of fact, these significant losses of tin loading in the synthesis process explain the difficulty for synthesizing materials with low Sn contents (Sn/Pd < 1). In contrary, XPS characterizations indicate an enrichment of tin at the surface, or at least in the first nanometer depth from the surface, of the materials, with respect to the bulk. Moreover, the surface atomic ratios are close to the nominal values, although the values tend to diverge a little bit from nominal values as the tin amount increases. It is worth to note that independently on the nominal Pd/Sn ratio, the surface enrichment by Sn does not affect the ratio between zero valence Sn (Sn^0) and oxide/hydroxide Sn species (SnO_xH_y), which remains about 20%/80%, respectively. This suggests that Sn^0 is in strong interaction with palladium, whereas SnO_xH_y species forms clusters at the Pd particle surface. Such structure was already proposed for PdBi, PdNi [6,9,17], and PtSn [22] systems. At last, the surface ratios as determined by XPS lead to values close to the desired ones for the bulk (nominal ones) in the case of catalysts with lower Sn contents (Pd_1Sn_1 and Pd_1Sn_2). The specific surface areas of Pd_1Sn_x were determined using the BET method. Materials have relatively high surface areas regarding their particle size, depending on the Sn contents. Values lying between 25 and 80 $m^2\,g^{-1}$ (Table 2) were

Table 2
Nominal atomic ratios, atomic ratios determined from atomic absorption measurements and from XPS characterizations, and real surface area determined by BET method of catalysts used in electrochemical experiments.

	PdSn	$PdSn_2$	$PdSn_3$
Nominal at %	50/50	33/66	25/75
Atomic absorption (AA) at %	66/34	61/39	56/44
XPS at %	48/52	35/65	31/69
Surface area ($m^2\,g^{-1}$)	25	30	77

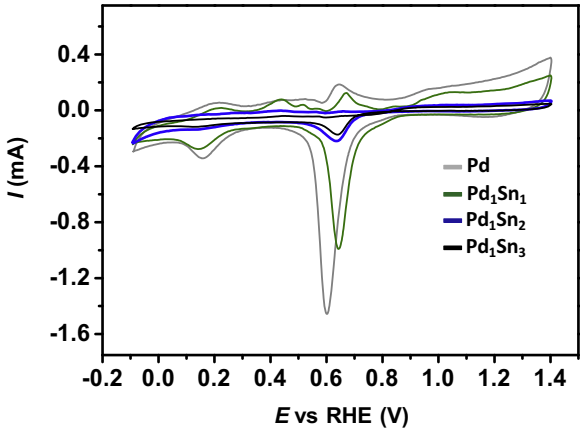

Fig. 3. Cyclic voltammograms of $PdSn_x$ self-supported catalysts recorded in 0.1 M KOH N_2-saturated electrolyte ($v = 0.020\ V\ s^{-1}$; $T = 25\ ^\circ C$).

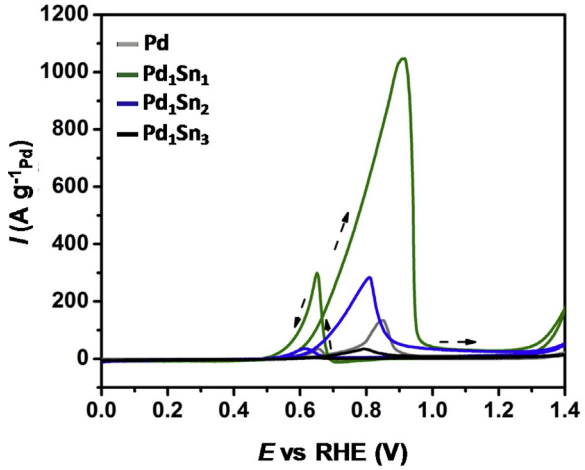

Fig. 4. Polarization curves recorded for the oxidation of 0.1 M Glycerol in 1 M KOH electrolyte on self-supported $PdSn_x$ catalysts at $0.020\ V\ s^{-1}$ ($T = 25\ ^\circ C$).

determined. These values increase with the Sn/Pd ratio. The leaching of the catalyst surface by the KOH treatment may be more important as the nominal ratio of tin is high, allowing a process comparable to a dealloying effect to occur, which leads to increase the real surface area.

The stable cyclic voltammograms of Pd_1Sn_x in supporting 0.1 M KOH electrolyte are presented in Fig. 3. The presence of tin does not modify the general shape of the voltammograms, only the intensities of current over the whole potential range are decreased. The drastic decrease of currents for hydrogen adsorption/desorption process and Pd surface oxide formation/reduction with the increase of the tin loading indicates that the Pd surface is more and more covered by tin species. The limitation of the hydrogen adsorption/desorption process was already observed for Pd nanoparticles modified by bismuth [8,9], but it was also accompanied with an increase of the oxide reduction peak intensity and with a shift toward lower potentials. Such behavior was explained in terms of strong interactions between Pd surface and Bi atoms. Here, the intensity of the surface oxide reduction peak in the 0.6–0.7 V range only decreases with the increase of Sn content; this peak is only due to the available Pd surface oxide reduction. Moreover, conversely to that observed in the case of PdBi system, this reduction peak is shifted toward higher potentials, which shows that the interactions between Pd and Sn and between Pd and Bi are different, so are their catalytic behaviors.

Polarization curves recorded on the Pd_1Sn_x catalysts in $1.0\ mol\ L^{-1}$ KOH + $0.1\ mol\ L^{-1}$ glycerol are presented in Fig. 4. The Pd_1Sn_1 material displays a very high activity in comparison with that recorded on a pure Pd catalyst, evidencing the beneficial effect of adding tin to palladium. The onset potential of glycerol oxidation is shifted from 0.6 V for pure Pd catalyst down to 0.45 V for the Pd_1Sn_1 catalyst. But when the Sn content in catalysts increases, the activity of catalysts toward the glycerol electrooxidation reaction decreases dramatically and even becomes lower than that obtained with pure Pd catalyst in the case of Pd_1Sn_3. The activity decrease with tin content in the catalytic material is explained in terms of palladium active surface coverage and availability of active sites for adsorbing glycerol molecules prior to their oxidation. At last, the performance of the Pd_1Sn_1 catalyst, reaching more than $1000\ A\ g_{Pd}^{-1}$ makes it one of the best catalysts for the glycerol electrooxidation reaction.

Chronoamperometry curves were recorded for 5000 s at 0.6 V in presence of 0.1 M glycerol on different Pd_1Sn_x catalysts (Fig. 5) and compared to that recorded on the pure Pd catalyst. The currents recorded on both Pd and Pd_1Sn_3 catalysts drop rapidly toward a value close to zero, whereas on the Pd_1Sn_2 and Pd_1Sn_1 catalysts the currents first decrease and then stabilize at *ca.* $10\ A\ g_{Pd}^{-1}$ and *ca.* $20\ A\ g_{Pd}^{-1}$, respectively; Pd_1Sn_1 is the most active one. For this latter material, after the initial current density of *ca.* $130\ A\ g_{Pd}^{-1}$, a dramatic drop of current down to *ca.* $45\ A\ g_{Pd}^{-1}$ occurs in a few seconds, likely related to capacitive current decay. Then a slow decrease and the stabilization of the activity at *ca.* $20\ A\ g_{Pd}^{-1}$ occurs, which is convenient with cyclic voltammetry measurements (Fig. 4). This behavior can be attributed to the formation of adsorbed species from glycerol at the surface of the catalyst leading to lower active surface area and lower glycerol oxidation activity until an equilibrium between adsorption of species from glycerol and desorption of reaction products is reached. The stabilization of the current is reached sooner with the Pd_1Sn_2 catalyst than with the Pd_1Sn_1 which could be due to a Sn/Pd surface ratio leading to a good balance between OH species from tin and species from glycerol adsorption on Pd; on the other hand, the lower activity of Pd_1Sn_2 can be due to the lower Pd surface exposed. These results not only highlight the higher activity of Sn containing catalysts, but also the good stability of the Pd_1Sn_1 material.

The selectivity of the Pd_1Sn_1 catalyst toward the glycerol electrooxidation reaction has been studied using *in situ* infrared reflection spectroscopy measurements. In the ATR–IRRAS configuration, positive absorption bands correspond to the formation of species and negative bands to the consumption of reactants or

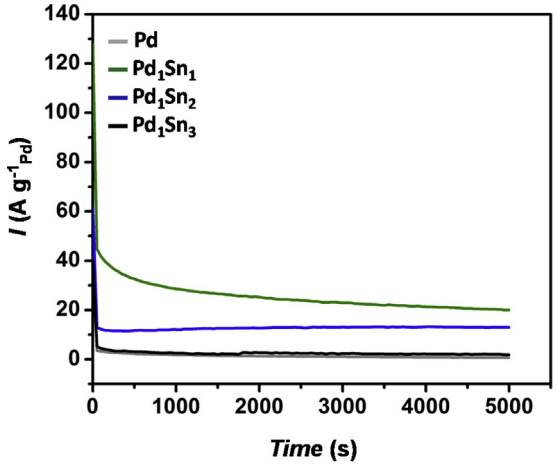

Fig. 5. Chronoamperometry recorded for the glycerol electro-oxidation on a self-supported Pd and $PdSn_x$ catalysts at 0.6 V *vs* RHE, in 1 M KOH + 0.1 M glycerol solution ($T = 25\ ^\circ C$).

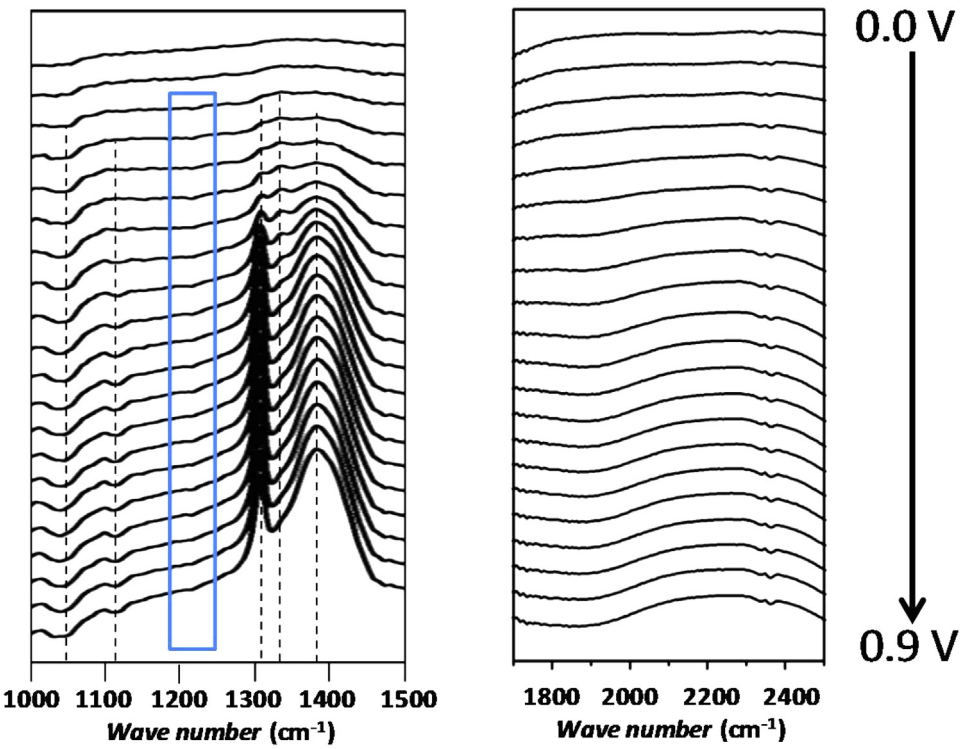

Fig. 6. *In situ* FTIR spectra recorded for the glycerol electrooxidation on a self-supported PdSn catalyst from 0.0 V *vs* RHE to 0.9 V *vs* RHE in 1 M KOH + 0.1 M glycerol solution (scan rate 0.001 V s^{-1}, $T = 25\,^{\circ}C$).

intermediates. The *in-situ* infrared spectra recorded on the Pd_1Sn_1 catalyst for the oxidation of 0.1 mol L^{-1} glycerol in 1.0 mol L^{-1} KOH electrolyte at a potential scan rate of 1 mV s^{-1} are presented in Fig. 6. The part of the spectra in the range from 1400 cm^{-1} to 1800 cm^{-1} was removed because the presence of water leads to IR absorption bands in this wavenumber region which superimpose with absorption bands of other species (such as carbonyl) [23,24] and make interpretation impossible. In the IR fingerprint region, from 1000 cm^{-1} to 1400 cm^{-1}, several absorption bands can be observed. The negative absorption bands located at *ca.* 1040 cm^{-1}, 1110 cm^{-1}, and 1225 cm^{-1} (with a very low intensity for the latter one), appearing at low electrode potentials (between 0.1 and 0.3 V) corresponds to the consumption of species. The first one at 1040 cm^{-1} is observable over the whole potential range where the catalyst is active for the oxidation of glycerol, and its intensity increases (in absolute value) as the potential is increased; this band can reasonably be assigned to the consumption of alcohol functions. The absorption bands at *ca.* 1110 cm^{-1} and 1225 cm^{-1} are appearing a little bit later than that at 1040 cm^{-1} (*ca.* 0.3 V and *ca.* 0.15 V, respectively) and have low intensities. They are assigned to the stretching mode of aldehyde or alcohol groups, 25 and can reasonably be attributed to the consumption of previously formed aldehyde species adsorbed at the electrode surface. The positive absorption bands located at *ca.* 1304 cm^{-1}, 1330 cm^{-1}, and 1380 cm^{-1} also appearing at low potentials on this catalyst (from *ca.* 0.15 V) are assigned to the formation of either glyceraldehyde or glycerate for the first one [9,25], to the formation of hydroxyacetone for the second one [9,25] and to the formation of carboxylate for the last one [9,25,26]. The ketone specie, dihydroxyacetone, is formed over the same potential range as the aldehyde specie, so that both these species are intermediates for the formation of carboxylate species, as it is attested by the simultaneous presence of the absorption bands at *ca.* 1304 cm^{-1} and 1380 cm^{-1}.

The wave number range from 1700 cm^{-1} to 2100 cm^{-1} corresponds to the region where the infrared signatures of adsorbed CO on palladium (*ca.* 1950 cm^{-1} and 2050 cm^{-1} for linearly bonded and bridge bonded CO_{ads}, respectively) [27] and of interfacial CO_2 (2043 cm^{-1}) [28] could be detected. No signal is present in the IR spectra over the whole studied potential range. The small double-band visible at *ca.* 2343 cm^{-1} could be considered as an evidence of the production of CO_2 on the catalyst. But this band appears as soon as 0.0 V, is visible over the whole potential range with a constant intensity and present a forbidden transition (it looks like a double band) characteristic of gas phase CO_2 [29], which is not the case for dissolved CO_2 [30]. This double band comes then from a purge weakness over the optical pathway of the infrared beam. Therefore, the Pd_1Sn_1 material does not catalyze the dissociative adsorption of glycerol with C—C bond breaking, as it was observed with self-supported PdBi catalysts [15]. This fact confirms the adsorption mode of glycerol leading to the formation of adsorbed aldehyde and/or ketone at the Pd_1Sn_1 catalyst surface, rather than adsorbed CO, as it was also shown with PtSn catalyst for ethanol oxidation in acidic medium [31].

4. Discussion

The Pd_1Sn_1 catalyst presents a very high initial activity at 0.6 V toward the glycerol elecrooxidation reaction, close or even higher to that recorded previously on a very active Pd_4Bi_1 catalyst [15]. Moreover, a current stabilization at *ca.* 20 A g^{-1} after 2 h chronoamperometry experiment was observed for both catalysts although Pd/Sn surface ratio was higher than Pd/Bi surface ratio. So that, either the available Pd surface is unchanged due to a smaller coverage by Sn species in comparison with Bi species, or the glycerol turnover is higher on Pd_1Sn_1 catalyst than on Pd_4Bi_1 catalyst.

Considering the selectivity studies using *in situ* infrared spectroscopy measurements, the presence at very low potentials of absorption bands at *ca.* 1310 cm^{-1} and 1380 cm^{-1} assigned to carboxylate groups, simultaneously to the formation of aldehyde and ketone species, indicates that the bifunctional mechanism [32] with

hydroxyl species activation by tin species occurs preferentially on the Pd_1Sn_1 material. The absence of the absorption band at *ca.* 1350 cm^{-1} attributed to the formation of hydroxypyruvate [6,24] whereas the absorption band attributed to the formation of dihydroxyacetone at *ca.* 1335 cm^{-1} is visible on the spectra, deserves a deeper explanation. Indeed, if dihydroxyacetone is first formed at the electrode, then the following step leading to higher oxidation level of the molecule toward compounds containing carboxylate groups should involve hydroxypyruvate as reaction intermediate, according to the following reactions:

$$H_2OH\text{-}CHOH\text{-}CH_2OH + 2OH^- \rightarrow (CH_2OH\text{-}CO\text{-}CH_2OH)_{ads} + 2H_2O + 2e^- \quad (1)$$

$$(CH_2OH\text{-}CO\text{-}CH_2OH)_{ads} + 5OH^- \rightarrow (CH_2OH\text{-}CO\text{-}COO^-)_{ads} + 4H_2O + 4e^- \quad (2)$$

$$(CH_2OH\text{-}CO\text{-}COO^-)_{ads} + 5OH^- \rightarrow COO^-\text{-}CO\text{-}COO^- + 4H_2O + 4e^- \quad (3)$$

The non-detection of hydroxyyruvate can be explained by a rapid isomerization reaction of dyhydroxyacetone into glyceraldhedyde. This isomerization reaction was already invoked in order to explain differences in glycerol oxidation mechanism as a function of composition and structure of Bi-modified Pt and Pd-based catalysts. Glyceraldehyde is then expected to oxidize very rapidly, particularly in presence of the very oxophilic tin metal, to give glycerate according to the following reactions:

$$CH_2OH\text{-}CHOH\text{-}CH_2OH + 2OH^- \rightarrow (CH_2OH\text{-}CO\text{-}CH_2OH)_{ads} + 2H_2O + 2e^- \quad (4)$$

$$(CH_2OH\text{-}CO\text{-}CH_2OH)_{ads} \rightleftarrows (CH_2OH\text{-}CHOH\text{-}CHO)_{ads} \quad (5)$$

$$(CH_2OH\text{-}CHOH\text{-}CHO)_{ads} + 3OH^- \rightarrow CH_2OH\text{-}CHOH\text{-}COO^- + 2H_2O + 2e^- \quad (6)$$

which can eventually be followed by,

$$CH_2OH\text{-}CHOH\text{-}COO^- + 5OH^- \rightarrow {}^-OOC\text{-}CHOH\text{-}COO^- + 4H_2O + 4e^- \quad (7)$$

and/or,

$$CH_2OH\text{-}CHOH\text{-}COO^- + 7OH- \rightarrow {}^-OOC\text{-}CO\text{-}COO^- + 6H_2O + 6e^- \quad (8)$$

The second possibility consists in considering the formation of hydroxypyruvate from dihydroxyacetone, followed be the rapid oxidation of hydroxypyruvate into mesoxalate. The high kinetics of hydroxypyruvate conversion would make very difficult, even impossible, its detection by *in situ* infrared spectroscopy. Here, it is assumed that the transformation of dihydroxyacetone into hydroxypyuvate is the limiting step of the whole oxidation reaction. This mechanism is not convincing for us. Indeed, in different works performed in our laboratories concerning glycerol electrooxidation mechanism in alkaline media, on carbon supported gold nanoparticles, Pd-based and Pd-based catalysts [6,9,17], on self-supported Pd_4Bi_1 catalysts [15] and on unsupported well shaped Pd nanoparticles modified by Bi [33], it was observed that each times hydroxypyruvate was formed, the productions of carbonate, CO_2 and other C1 and C2 compounds occurred almost simultaneously. However, in the case of the self-supported Pd_1Sn_1 catalyst, no evidence of the formation of C1 and C2 compounds, particularly the unique signatures of bridge bonded CO_{ads}, of CO_3^{2-} and of CO_2 at *ca.* 1950 cm^{-1}, 1410 cm^{-1} and 2343 cm^{-1} [26,27,28], respectively, is observed; the self-supported Pd_1Sn_1 catalyst does not activate the C—C bond cleavage, conversely to that was observed with a self-supported Pd_4Bi_1 catalysts. The other consequence of this remark is that the isomerization reaction of dihydroxyacetone into glyceraldehyde preferentially occurs, allowing further oxidation reaction toward carboxylates with high kinetics. It is moreover well known that in the case of ethanol electrooxidation in acidic medium the modification of the catalytic noble metal by tin highly limit the formation of acetaldehyde at the expense of the production of acetic acid [11], thanks to the bifunctional mechanism where tin provides the activated oxygenated species to complete the oxidation reaction into acid carboxylic form. It is likely that the same successive reactions occurs with glycerol oxidation on Pd_1Sn_1: following the example of acetaldehyde, glyceraldehyde formed by the isomerization reaction of dihydroxyacetone is likely very reactive (aldehyde are not very stable in alkaline medium) [34] moreover in the presence of oxophilic tin species at the surface of the catalyst, and is then rapidly transformed into glycerate and further into higher C3 oxidation compounds.

All these remarks shows that self-supported Pd_1Sn_1 catalyst is very active for glycerol electrooxidation and very selective toward C3 carboxylate compounds which are very important platform chemicals for industrial applications [35,36].

5. Conclusion

A series of active Pd_1Sn_x catalysts with high Sn atomic ratios (≥50%) were synthesized by the combination of the Sacrificial support method and a thermal reduction process. Self-supported Pd_1Sn_x catalysts have porous morphologies corresponding to beads of agglomerated *ca.* 20 nm nanoparticles delimiting pores of several tenth nanometer diameters. Such structure leads to surface areas ranging from 25 to 80 $m^2\ g^{-1}$, depending on the Sn content. Pd_1Sn_1 and Pd_1Sn_2 catalysts displayed higher activity toward glycerol oxidation, confirming the promotion effect of tin, but the Pd_1Sn_1 one was found to be the most active. The most important highlights are the following:

- The modification of Pd by Sn decreases the onset potential for glycerol oxidation from 0.6 V for pure Pd down to 0.45 V for Pd_1Sn_1.
- Conversely to what was previously observed with bismuth, the modification of Pd by Sn favors the bifunctional mechanism toward the formation of carboxylate species at low potentials, from the onset potential of the oxidation wave;
- The presence of Sn annihilates the ability of palladium to activate the dissociative adsorption of glycerol with C—C bond breaking and suppress the formation of CO_3^{2-} and CO_2,
- Self-supported Pd_1Sn_1 is a very active and selective catalyst for the production of C3 carboxylate compounds, which are of paramount interest as platform chemicals for industrial applications.

This work represents then an important demonstration that the combination of the control of the catalyst composition/morphology/structure allows orientating selectively the

oxidation of alcohols, particularly glycerol, toward a given valuable product family for electro-synthesis application.

Acknowledgements

Anna Zalineeva thanks the Center for Emerging Energy Technologies, Farris Engineering Center (UNM) for assistance and technical support, and the County Council of Poitou-Charentes (France) for financial support.

References

[1] M.A. Dasari, P.P. Kiatsimkul, W.R. Sutterlin, G.J. Suppes, Appl. Catal. A 281 (2005) 225–231.
[2] J.M. Clacens, Y. Pouilloux, J. Barrault, Appl. Catal. A 227 (2002) 181–190.
[3] M. Simoes, S. Baranton, C. Coutanceau, ChemSusChem 5 (2012) 2106–2124.
[4] C. Bianchini, P.K. Shen, Chem. Rev. 109 (2009) 4183–4206.
[5] N. Tian, Z.-Y. Zhou, N.-F. Yu, L.-Y. Wang, S.-G. Sun, J. Am. Chem. Soc. 132 (2010) 7580–7581.
[6] M. Simoes, S. Baranton, C. Coutanceau, Appl. Catal. B: Environ. 93 (2010) 354–362.
[7] V. Bambagioni, C. Bianchini, A. Marchionni, J. Filippi, F. Vizza, J. Teddy, P. Serp, M. Zhiani, J. Power Sources 190 (2009) 241–251.
[8] I.G. Casella, M. Contursi, Electrochim. Acta 52 (2006) 649–657.
[9] M. Simoes, S. Baranton, C. Coutanceau, Appl. Catal. B: Environ. 110 (2011) 40–49.
[10] A. Serov, U. Martinez, P. Atanassov, Electrochem. Commun. 34 (2013) 185–188.
[11] S. Rousseau, C. Coutanceau, C. Lamy, J.M. Léger, J. Power Sources 158 (2006) 18–24.
[12] R. Awasthi, R.N. Singh, Int. J. Hydrogen Energy 37 (2012) 2103–2110.
[13] R.M. Modibedi, T. Masombuka, M.K. Mathe, Int. J. Hydrogen Energy 36 (2011) 4664–4672.
[14] T. Ramulifho, K.I. Ozoemena, R.M. Modibedi, C.J. Jafta, M.K. Mathe, J. Electroanal. Chem. 692 (2013) 26–30.
[15] A. Zalineeva, M. Padilla, U. Martinez, A. Serov, K. Artyushkova, S. Baranton, C. Coutanceau, P.B. Atanassov, J. Am. Chem. Soc. 136 (2014) 3937–3945.
[16] A. Serov, M.H. Robson, K. Artyushkova, P. Atanassov, Appl. Catal. B 127 (2012) 300–306.
[17] M. Simoes, Thèse de Doctorat, Université de Poitiers, Poitiers (France), 2011.
[18] A. Serov, M.H. Robson, B. Halevi, K. Artyushkova, P. Atanassov, Electrochem. Commun. 22 (2012) 53–56.
[19] A. Serov, M.H. Robson, M. Smolnik, P. Atanassov, Electrochim. Acta 109 (2013) 433–439.
[20] C.D. Wagner, W.M. Riggs, L.E. Davis, J.F. Moulder, G.E. Mouilenberg (Eds.), Handbook of Xray Photoelectron Spectroscopy, PerkinElmer Corporation, Eden Prairie, MN, 1978, p. 1.
[21] W. Du, K.E. Mackenzie, D.F. Milano, N.A. Deskins, D. Su, X. Teng, ACS Catal. 2 (2012) 287–297.
[22] S. Beyhan, S. Pronier, Mater. Res. Bull. 50 (2014) 246–248.
[23] X.H. Xia, H.-D. Liess, T. Iwasita, J. Electroanal. Chem. 437 (1997) 233–240.
[24] F. Vigier, C. Coutanceau, F. Hahn, E.M. Belgsir, C. Lamy, J. Electroanal. Chem. 563 (2004) 81–89.
[25] C.J. Pouchert, The Aldrich Library of Infrared Spectra, third edition, Aldrich Chemical Company, Inc., Milwaukee, WI, USA, 1981.
[26] P.A. Christensen, A. Hamnet, J. Electroanal. Chem. 260 (1989) 347–359.
[27] Y.-X. Jiang, S.-G. Sun, N. Ding, Chem. Phys. Lett. 344 (2001) 463–470.
[28] R.B. de Lima, V. Paganin, T. Iwasita, W. Vielstich, Electrochim. Acta 49 (2003) 85–91.
[29] M.B. Esler, D.W.T. Griffith, S.R. Wilson, L.P. Steele, Anal. Chem. 72 (2000) 216–221.
[30] M.K. Nieuwoudt, M.P. Simpson, M. Tobin, L. Puskar, Vib. Spectrosc. 75 (2014) 136–148.
[31] J.M. Léger, S. Rousseau, C. Coutanceau, F. Hahn, C. Lamy, Electrochim. Acta 50 (2005) 5118–5125.
[32] M. Watanabe, S. Motoo, J. Electroanal. Chem. 60 (1975) 275–283.
[33] A. Zalineeva, Thèse de Doctorat, Université de Poitiers, Poitiers (France), 2014.
[34] Y. Kwon, S.C.S. Lai, P. Rodriguez, M.T.M. Koper, J. Am. Chem. Soc. 133 (2011) 6914–6917.
[35] P. Gallezot, Catal. Today 37 (1997) 405–418.
[36] A. Behr, J. Eilting, K. Irawadi, J. Leschinski, F. Lindner, Green Chem. 10 (2008) 13–30.